Journal of Computational and Applied Mathematics 264 (2014) 49–64

Contents lists available at ScienceDirect

Journal of Computational and Applied Mathematics

journal homepage: www.elsevier.com/locate/cam

On the numerical solution of two-phase Stefan problems with heat-flux boundary conditions

S.L. Mitchell *, M. Vynnycky

Mathematics Applications Consortium for Science and Industry (MACSI), Department of Mathematics and Statistics, University of Limerick, Limerick, Ireland

ARTICLE INFO

Article history:
Received 22 April 2013
Received in revised form 17 October 2013

Keywords:
Stefan problem
Keller box scheme
Boundary immobilization
Starting solutions
Two-phase

ABSTRACT

A recently derived numerical algorithm for one-dimensional one-phase Stefan problems is extended for the purpose of two-phase moving boundary problems in which the second phase first appears only after a finite delay time; this can occur if the phase change is caused by a heat-flux boundary condition. In tandem with the Keller box finite-difference scheme, the so-called boundary immobilization method is used. An important component of the work is the use of variable transformations that must be built into the numerical algorithm to resolve the boundary-condition discontinuity that is associated with the onset of phase change. This allows the delay time until solidification begins to be determined, and gives second-order accuracy in both time and space.

1. Introduction

Phase-change, or Stefan, problems in which a material melts or solidifies occur in a wide variety of natural and industrial processes. Mathematically, these are special cases of moving-boundary problems, in which the location of the front between the solid and liquid is not known beforehand, but must be determined as part of the solution. Although most activity has been devoted to the classical one-dimensional Stefan problem in which phase change occurs due to a constant heating or cooling temperature, of more practical relevance is the situation where a heat flux or convective boundary condition is imposed. In general, there are no analytical solutions available for these cases and thus numerical methods are necessary. Furthermore, of all the numerical methods that have been applied to the classical problem, only the heat balance integral method has been extended to the non-classical Stefan problem [1–6]. Whilst this method is popular, an unsatisfactory feature is the use of assumptions on the form of the solution that may not be generally valid; furthermore, the solution obtained is of indeterminate order of accuracy. Amongst the other available numerical methods, the boundary immobilization method, implemented in tandem with the Keller Box scheme, has recently emerged as the most accurate alternative for the classical problem [7], and the purpose of this paper is to demonstrate the use of this method for the non-classical problem.

There are, however, several obstacles which make the extension non-trivial. Unlike the problems analysed in [7], which considered a material that was initially at its melting temperature, phase change will not commence instantaneously if the material is not at this temperature, and a central part of the problem is to determine when this actually occurs. Thereafter, it is necessary to determine the location of the moving phase-change boundary and, as in [7], to consider how numerically to handle the new phase, given that its thickness is initially zero. An initial analysis of the problem was undertaken in [8], and a principal finding was that the phase-change front starts to grow as $(t - t_m)^{3/2}$, where t_m is the time taken for phase change to begin; although similar to that for ablation problems [9], the initial evolution of the front is different to that for the classical Stefan problem, which has behaviour $(t - t_m)^{1/2}$, with $t_m = 0$. However, the analysis in [8] was incomplete in several respects:

* Corresponding author.
E-mail addresses: sarah.mitchell@ul.ie, sarahmitc@gmail.com (S.L. Mitchell).

0377-0427/$ – see front matter © 2014 Elsevier B.V. All rights reserved.
http://dx.doi.org/10.1016/j.cam.2014.01.003

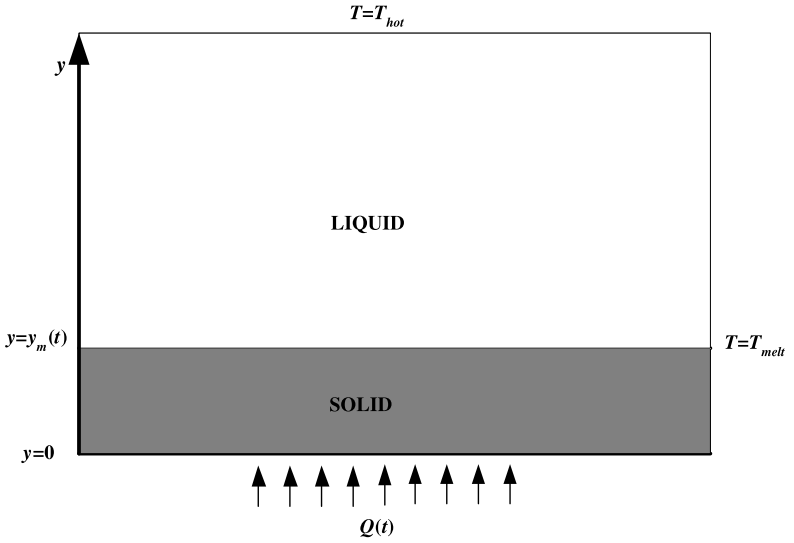

Fig. 1. System geometry.

1. the numerical scheme was not able to compute when phase change began;
2. no numerical scheme was given for the entire problem, only for the phase-change stage, and even this was only possible because an analytical expression was available for the initial condition for this stage;
3. the formal accuracy of the numerical scheme was not verified.

The layout of the paper is as follows. In Section 2, we formulate a problem for the solidification, due to a cooling heat flux, of material that is initially above its melting temperature; in Section 3, we nondimensionalize the model equations and transform them to a form more suitable for numerical integration. In Section 4, we explain how the Keller box scheme, in tandem with the boundary immobilization method, is applied to this particular problem. The results are then presented and discussed in Section 5, and conclusions are drawn in Section 6.

2. Mathematical formulation

Consider the cooling of a liquid, occupying the half-plane $y > 0$, that is initially at a temperature, T_{hot}, which is greater than its melting temperature, T_{melt}, and which is cooled at $y = 0$ for time $t > 0$ by an applied heat flux $Q(t)$. After cooling commences, the temperature of the liquid decreases until some time t_m, at which stage solid begins to form at $y = 0$; subsequently, solid occupies the region $0 \leq y \leq y_m(t)$ and liquid occupies $y > y_m(t)$, where $y_m(t)$ denotes the location of the solidification front. A schematic is shown in Fig. 1.

Assuming the material properties of the solid and liquid phases to be constant, the governing equations are as follows. For $0 < t < t_m$ and $y > 0$, and then $t > t_m$ and $y > y_m(t)$, we have

$$\rho_l c_{pl} \frac{\partial T_l}{\partial t} = k_l \frac{\partial^2 T_l}{\partial y^2}, \tag{1}$$

where T_l is the liquid temperature, k_l is the thermal conductivity of the liquid, c_{pl} is its specific heat capacity and ρ_l its density. For $t > t_m$ and $0 < y < y_m(t)$, we have

$$\rho_s c_{ps} \frac{\partial T_s}{\partial t} = k_s \frac{\partial^2 T_s}{\partial y^2}, \tag{2}$$

where T_s is the solid temperature, k_s is the thermal conductivity of the solid, c_{ps} is its specific heat capacity and ρ_s its density. We assume henceforth that $\rho_l = \rho_s = \rho$.

For boundary conditions, we have, at $y = y_m(t)$,

$$T_s = T_l = T_{melt}, \tag{3}$$

and the Stefan condition,

$$k_s \frac{\partial T_s}{\partial y} - k_l \frac{\partial T_l}{\partial y} = \rho \Delta H_f \frac{\mathrm{d}y_m}{\mathrm{d}t}, \tag{4}$$

where ΔH_f is the latent heat of fusion. At $y = 0$, we have

$$\begin{cases} k_l \dfrac{\partial T_l}{\partial y} = Q\,(t) & \text{for } 0 \le t \le t_m, \\ k_s \dfrac{\partial T_s}{\partial y} = Q\,(t) & \text{for } t > t_m, \end{cases} \tag{5}$$

where $Q\,(t) > 0$. Also, as $y \to \infty$, we have

$$T_l \to T_{hot}. \tag{6}$$

Since Eq. (1) is a parabolic partial differential equation, it requires an initial condition; for this, we take

$$T_l = T_{hot} \quad \text{at } t = 0. \tag{7}$$

An initial condition is also required for (2), although this cannot be set at $t = 0$ since there is initially no solid; instead this must be set at $t = t_m$, i.e. when solid first appears. Hence, for T_s we take

$$T_s = T_{melt} \quad \text{at } t = t_m; \tag{8}$$

in addition, we must have

$$y_m(t_m) = 0. \tag{9}$$

3. Nondimensionalization

It is more convenient to proceed in nondimensional variables. To do this, we write

$$\tilde{y} = \frac{y}{[y]}, \qquad \tilde{y}_m = \frac{y_m}{[y]}, \qquad \tilde{t} = \frac{t}{[t]}, \qquad \tilde{T}_{l,s} = \frac{T_{melt} - T_{l,s}}{\Delta T}, \qquad \mathcal{Q} = \frac{Q}{[Q]}, \qquad \tilde{t}_m = \frac{t_m}{[t]}, \tag{10}$$

where $\Delta T = T_{hot} - T_{melt}$, $[Q]$ is a heat flux scale and $[y]$ and $[t]$ are length and time scales, respectively; the latter two are to be determined. We choose these from the pre-solidification phase by taking $[t]$ from the heat equation (1) and $[y]$ from the boundary condition (5); this gives

$$[t] = \frac{\rho c_{pl} [y]^2}{k_l}, \qquad [y] = \frac{k_l \Delta T}{[Q]}. \tag{11}$$

After dropping the tildes, Eqs. (1) and (2) then become

$$\frac{\partial T_l}{\partial t} = \frac{\partial^2 T_l}{\partial y^2}, \tag{12}$$

$$\kappa \frac{\partial T_s}{\partial t} = \frac{\partial^2 T_s}{\partial y^2}, \tag{13}$$

respectively, where $\kappa = c_{ps} k_l / c_{pl} k_s$. The boundary conditions for T_l and T_s are then

$$T_s = T_l = 0 \quad \text{at } y = y_m(t), \tag{14}$$

$$\beta \frac{\mathrm{d}y_m}{\mathrm{d}t} = \frac{\partial T_l}{\partial y} - K \frac{\partial T_s}{\partial y} \quad \text{at } y = y_m(t), \tag{15}$$

$$\frac{\partial T_l}{\partial y} = -\mathcal{Q}\,(t) \quad \text{at } y = 0, \text{ for } 0 \le t \le t_m, \tag{16}$$

$$K \frac{\partial T_s}{\partial y} = -\mathcal{Q}\,(t) \quad \text{at } y = 0, \text{ for } t > t_m \tag{17}$$

$$T_l \to -1 \quad \text{as } y \to \infty, \tag{18}$$

where $K = k_s / k_l$ and $\beta = \Delta H_f / [c_{pl} \Delta T]$ is the inverse Stefan number. The initial conditions (8) and (9) are, respectively,

$$T_l = -1 \quad \text{at } t = 0, \tag{19}$$

$$T_s = 0 \quad \text{at } t = t_m, \tag{20}$$

$$y_m(t_m) = 0. \tag{21}$$

Observe that $T_l < 0$ for $0 < t < t_m$, and so t_m is determined as the nondimensional time when $T_l(0, t)$ reaches 0.

In order to facilitate the verification of our numerical scheme later on, we choose $\mathcal{Q}(t)$ so that there is at least an analytical solution in the pre-solidification stage; it is evidently not possible to choose $\mathcal{Q}(t)$ so that there is an analytical solution in the solidification stage also. In particular, we will take $\mathcal{Q}(t) = 1$. Note that if $\mathcal{Q}(t)$ is taken to be of the form t^{α}, where α is a real number, then it will still be possible to reduce Eq. (12) to an ordinary differential equation, as happens when we take $\mathcal{Q}(t) = 1$; for physically realistic solutions, in the sense that T is not infinite at $t = 0$, we would need $\alpha > -1/2$. Otherwise, if $\mathcal{Q}(t)$ is not of the form t^{a}, it would be necessary to solve for T_l numerically; in this case, the method we present later in Section 4 can be used.

In consequence, with $\mathcal{Q}(t) = 1$, we have

$$T_l(y, t) = -1 + 2\sqrt{\frac{t}{\pi}}\exp\left(-\frac{y^2}{4t}\right) - y\,\mathrm{erfc}\left(\frac{y}{2\sqrt{t}}\right), \tag{22}$$

and, in turn, we obtain $t_m = \pi/4$. Ultimately, we will require our numerical scheme to be able to compute t_m, and to this end we set $\zeta = t/t_m$, so that t_m appears in the governing equations. Then, in the pre-solidification stage, we solve

$$\frac{\partial T_l}{\partial \zeta} = t_m \frac{\partial^2 T_l}{\partial y^2}, \quad y > 0, 0 < \zeta < 1, \tag{23}$$

with boundary conditions

$$\frac{\partial T_l}{\partial y} = -1 \quad \text{at } y = 0, \tag{24}$$

$$T_l \to -1 \quad \text{as } y \to \infty, \tag{25}$$

and initial condition

$$T_l = -1 \quad \text{at } \zeta = 0. \tag{26}$$

In addition, we have the condition

$$T_l(0, 1) = 0, \tag{27}$$

which will allow us to determine t_m.

The equations for the solidification stage, $\zeta > 1$, are

$$\frac{\partial T_l}{\partial \zeta} = t_m \frac{\partial^2 T_l}{\partial y^2}, \quad 0 < y < y_m(\zeta), \tag{28}$$

$$\kappa \frac{\partial T_s}{\partial \zeta} = t_m \frac{\partial^2 T_s}{\partial y^2}, \quad y > y_m(\zeta), \tag{29}$$

with boundary conditions

$$T_s = T_l = 0 \quad \text{at } y = y_m(\zeta), \tag{30}$$

$$\beta t_m^{-1} \frac{\mathrm{d}y_m}{\mathrm{d}\zeta} = \frac{\partial T_l}{\partial y} - K\frac{\partial T_s}{\partial y} \quad \text{at } y = y_m(\zeta), \tag{31}$$

$$K\frac{\partial T_s}{\partial y} = -1 \quad \text{at } y = 0, \tag{32}$$

$$T_l \to -1 \quad \text{as } y \to \infty, \tag{33}$$

and initial conditions

$$T_s(y, 1) = 0, \tag{34}$$

$$y_m(1) = 0, \tag{35}$$

$$T_l \equiv T_l(y, 1), \tag{36}$$

the latter being taken from the pre-solidification stage.

4. Numerical method

4.1. Discussion

As in [7,9,10], we focus on developing a numerical scheme centred on the Keller Box method, in tandem with transformed variables and the boundary immobilization method. We begin with the pre-solidification stage.

4.1.1. Pre-solidification stage

As pointed out in [10], and reiterated in [9], using a Keller Box scheme to solve an equation such as (23) in y and t variables will not give second-order accuracy for either the dependent variable, T_l, or its derivative with respect to y; the reason for this is that there is an inconsistency, or discontinuity, for $\partial T_l/\partial y$ near $(0, 0)$, since

$$\frac{\partial T_l}{\partial y}(y, 0) \to 0 \quad \text{as } y \to 0, \qquad \frac{\partial T_l}{\partial y}(0, t) = -1 \quad \text{as } t \to 0, \tag{37}$$

although note that there is no inconsistency for T_l, since

$$T_l(y, 0) \to -1 \quad \text{as } y \to 0, \qquad T_l(0, t) = -1 \quad \text{as } t \to 0. \tag{38}$$

To avoid this difficulty, we must transform variables via

$$z = \frac{y}{\sqrt{\zeta}}, \qquad \bar{\zeta} = \sqrt{\zeta}, \qquad T_l(y, \zeta) = -1 + \bar{\zeta}\theta_l(z, \bar{\zeta}); \tag{39}$$

Eqs. (23)–(25) then become

$$t_m \frac{\partial^2 \theta_l}{\partial z^2} = \frac{1}{2}\left(\theta_l + \bar{\zeta}\frac{\partial \theta_l}{\partial \bar{\zeta}}\right) - \frac{z}{2}\frac{\partial \theta_l}{\partial z}, \quad z > 0, 0 < \bar{\zeta} < 1, \tag{40}$$

$$\frac{\partial \theta_l}{\partial z} = -1 \quad \text{at } z = 0, \tag{41}$$

$$\theta_l \to 0 \quad \text{as } z \to \infty. \tag{42}$$

To obtain a starting solution we consider the limit as $\bar{\zeta} \to 0$; here, Eq. (40) reduces to

$$t_m \frac{\mathrm{d}^2 \theta_l}{\mathrm{d}z^2} = \frac{1}{2}\theta_l - \frac{z}{2}\frac{\mathrm{d}\theta_l}{\mathrm{d}z}, \tag{43}$$

which can be solved, along with the boundary conditions in (41), to give

$$\theta_l(z) = 2\sqrt{\frac{t_m}{\pi}}\exp\left(-\frac{z^2}{4t_m}\right) - z\,\mathrm{erfc}\left(\frac{z}{2\sqrt{t_m}}\right), \tag{44}$$

as the initial condition for (40). The extra condition (27) is now

$$\theta_l(0, 1) = 1. \tag{45}$$

Solving Eq. (40) numerically with the box scheme will give second-order accuracy for θ_l and $\partial\theta_l/\partial z$. However, it turns out that the solution for the solidification stage will require $\partial^2\theta_l/\partial z^2$ and $\partial^3\theta_l/\partial z^3$ at $\bar{\zeta} = 1$ as input; hence, we require second-order accuracy for those also, and it is then necessary to solve two auxiliary problems in order to find these higher order derivatives. Setting $U_l = \partial\theta_l/\partial z$ and $V_l = \partial U_l/\partial z$, we have

$$t_m \frac{\partial^2 U_l}{\partial z^2} = \frac{1}{2}\bar{\zeta}\frac{\partial U_l}{\partial \bar{\zeta}} - \frac{z}{2}\frac{\partial U_l}{\partial z}, \quad z > 0, 0 < \bar{\zeta} < 1 \tag{46}$$

$$U_l = -1 \quad \text{at } z = 0, \tag{47}$$

$$U_l \to 0 \quad \text{as } z \to \infty, \tag{48}$$

$$U_l = -\mathrm{erfc}\left(\frac{z}{2\sqrt{t_m}}\right) \quad \text{at } \bar{\zeta} = 0, \tag{49}$$

and

$$t_m \frac{\partial^2 V_l}{\partial z^2} = \frac{1}{2}\bar{\zeta}\frac{\partial V_l}{\partial \bar{\zeta}} - \frac{1}{2}V_l - \frac{z}{2}\frac{\partial V_l}{\partial z}, \quad z > 0, 0 < \bar{\zeta} < 1, \tag{50}$$

$$\frac{\partial V_l}{\partial z} = 0 \quad \text{at } z = 0, \tag{51}$$

$$V_l \to 0 \quad \text{as } z \to \infty, \tag{52}$$

$$V_l = \frac{1}{\sqrt{\pi t_m}}\exp\left(-\frac{z^2}{4t_m}\right) \quad \text{at } \bar{\zeta} = 0. \tag{53}$$

Note that (51) has been obtained from observing that since $U_l(0, \bar{\zeta}) = -1$, $\frac{\partial U_l}{\partial \bar{\zeta}}(0, \bar{\zeta}) = 0$; substituting this into (46) then gives the required result.

We define

$$g(z) := \theta_l(z, 1) = 2\sqrt{\frac{t_m}{\pi}}\exp\left(-\frac{z^2}{4t_m}\right) - z\,\mathrm{erfc}\left(\frac{z}{2\sqrt{t_m}}\right), \tag{54}$$

whence we will also have $g'(z) = U_l(z, 1), g''(z) = V_l(z, 1), g'''(z) = \partial V_l/\partial z(z, 1)$, where the prime denotes differentiation with respect to z; these will be required in the analysis below.

4.1.2. Solidification stage

For this stage, we set $\tau = \zeta - 1$ and

$$\xi = \begin{cases} y/y_m, & \text{for } y < y_m \\ y - y_m, & \text{for } y \geq y_m, \end{cases} \tag{55}$$

with

$$T_s(y, \zeta) = y_m F_s(\xi, \tau), \quad 0 \leq \xi < 1, \tau > 0, \tag{56}$$

$$T_l(y, \zeta) = F_l(\xi, \tau), \quad 0 \leq \xi < \infty, \tau > 0; \tag{57}$$

note that, in the pre-solidification phase, $\xi = y$ at $\zeta = 1$, which is consistent with the second line in (55), because $y_m = 0$ at $\zeta = 1$. Then, we have

$$t_m\frac{\partial^2 F_s}{\partial \xi^2} = \kappa y_m\left[\dot{y}_m F_s + y_m\frac{\partial F_s}{\partial \tau} - \xi\dot{y}_m\frac{\partial F_s}{\partial \xi}\right], \quad \text{for } 0 < \xi < 1, \tag{58}$$

$$t_m\frac{\partial^2 F_l}{\partial \xi^2} = \frac{\partial F_l}{\partial \tau} - \dot{y}_m\frac{\partial F_l}{\partial \xi}, \quad \text{for } 0 < \xi < \infty, \tag{59}$$

where the dot denotes differentiation with respect to τ; these are subject to

$$F_s|_{\xi=1} = F_l|_{\xi=0} = 0, \tag{60}$$

$$\beta t_m^{-1}\dot{y}_m = \left.\frac{\partial F_l}{\partial \xi}\right|_{\xi=0} - K\left.\frac{\partial F_s}{\partial \xi}\right|_{\xi=1}, \tag{61}$$

$$K\frac{\partial F_s}{\partial \xi} = -1 \quad \text{at } \xi = 0, \tag{62}$$

$$F_l \to -1 \quad \text{as } \xi \to \infty, \tag{63}$$

$$y_m = 0, \qquad F_l = -1 + g(\xi) \quad \text{at } \tau = 0. \tag{64}$$

The initial condition for F_l in (64) comes from the fact that $\theta_l(y, \zeta) = -1 + \bar{\zeta}T_l(\xi, \bar{\zeta})$ and so $F_l(\xi, 0) = -1 + T_l(\xi, 1) = -1 + g(\xi)$. Although $g \equiv g(z)$ from the pre-solidification stage, since $z = y/\zeta$ and $\xi = y - y_m$, it follows that $z = \xi$ at the start of the solidification stage.

How to proceed now is governed by the fact that $y_m \sim (t - t_m)^{3/2}$ as $t \to t_m$ or, equivalently, $y_m \sim \tau^{3/2}$ as $\tau \to 0$; this was shown in [8], and that analysis is re-capped in the Appendix. This means that, as $\tau \to 0$, Eq. (61) reduces to

$$\left.\frac{\partial F_l}{\partial \xi}\right|_{\xi=0} = K\left.\frac{\partial F_s}{\partial \xi}\right|_{\xi=1},$$

which implies that there is no inconsistency in either F_l or $\partial F_l/\partial \xi$ as $\tau, \xi \to 0$. The situation is therefore akin to that in [9], where it was demonstrated that it was in fact necessary to *introduce* an inconsistency in order to obtain a numerical scheme that is second-order accurate. Following [9], we reformulate the problem in terms of the ξ-derivatives of F_s and F_l. Setting

$$G_s := \frac{\partial F_s}{\partial \xi}, \qquad G_l := \frac{\partial F_l}{\partial \xi}, \tag{65}$$

Eqs. (58)–(64) become

$$t_m\frac{\partial^2 G_s}{\partial \xi^2} = \kappa y_m\left[y_m\frac{\partial G_s}{\partial \tau} - \xi\dot{y}_m\frac{\partial G_s}{\partial \xi}\right], \quad \text{for } 0 < \xi < 1, \tag{66}$$

$$t_m\frac{\partial^2 G_l}{\partial \xi^2} = \frac{\partial G_l}{\partial \tau} - \dot{y}_m\frac{\partial G_l}{\partial \xi}, \quad \text{for } 0 < \xi < \infty, \tag{67}$$

subject to

$$t_m \frac{\partial G_s}{\partial \xi}\bigg|_{\xi=1} = -\kappa y_m \dot{y}_m G_s x|_{\xi=1}, \qquad t_m \frac{\partial G_l}{\partial \xi}\bigg|_{\xi=0} = -\dot{y}_m G_l|_{\xi=0}, \tag{68}$$

$$\beta t_m^{-1} \dot{y}_m = G_l|_{\xi=0} - KG_s|_{\xi=1}, \tag{69}$$

$$KG_s = -1 \quad \text{at } \xi = 0, \tag{70}$$

$$G_l \to 0 \quad \text{as } \xi \to \infty, \tag{71}$$

$$y_m = 0, \qquad G_l = g'(\xi) \quad \text{at } \tau = 0. \tag{72}$$

Note that the equations in (68) have been obtained by observing that, since $F_s(1,\tau) = F_l(0,\tau) = 0$, it follows that $\frac{\partial F_s}{\partial \tau}(1,\tau) = \frac{\partial F_l}{\partial \tau}(0,\tau) = 0$; then, we make use of (58) and (59).

Next, we subtract off the initial condition by setting

$$\mathcal{G}(\xi,\tau) = G_l(\xi,\tau) - g'(\xi). \tag{73}$$

This gives, only rewriting equations involving the liquid,

$$t_m \frac{\partial^2 \mathcal{G}}{\partial \xi^2} = \frac{\partial \mathcal{G}}{\partial \tau} - \dot{y}_m \frac{\partial \mathcal{G}}{\partial \xi} - \dot{y}_m g''(\xi) - t_m g'''(\xi), \quad 0 < \xi < \infty, \tag{74}$$

$$\mathcal{G} \to 0 \quad \text{as } \xi \to \infty, \tag{75}$$

$$t_m \frac{\partial \mathcal{G}}{\partial \xi}\bigg|_{\xi=0} = -\dot{y}_m \mathcal{G}|_{\xi=0} - \dot{y}_m g'(0) - t_m g''(0), \qquad \beta t_m^{-1} \dot{y}_m = \mathcal{G}|_{\xi=0} - 1 - KG_s|_{\xi=1}, \tag{76}$$

$$\mathcal{G} = 0 \quad \text{at } \tau = 0. \tag{77}$$

Note here the significance of (73): it ensures that a starting similarity solution can be found to (74)–(77), as shown below. Without the substitution, it would be necessary to treat (67) numerically using a double-deck integration scheme, as implemented in [11] and discussed in [9,10], which is an altogether more cumbersome task; observe also the appearance in (74) of $g''(\xi)$ and $g'''(\xi)$, which explains why it was necessary to determine $\partial^2\theta_l/\partial z^2$ and $\partial^3\theta_l/\partial z^3$ earlier. In view of the inconsistency in $\partial\mathcal{G}/\partial\xi$ and the appearance of $\tau^{1/2}$ through $\dot{y}_m$, we set

$$\eta = \frac{\xi}{\tau^{1/2}}, \qquad \bar{\tau} = \tau^{1/2}, \qquad \mathcal{G}(\xi,\tau) = \bar{\tau} H_l(\eta,\bar{\tau}).$$

Then, Eqs. (66) and (74) become

$$t_m \bar{\tau} \frac{\partial^2 G_s}{\partial \xi^2} = \kappa y_m \left[\frac{1}{2} y_m \frac{\partial G_s}{\partial \bar{\tau}} - \frac{\xi}{2} \dot{y}_m \frac{\partial G_s}{\partial \xi}\right], \quad \text{for } 0 < \xi < 1, \tag{78}$$

$$t_m \frac{\partial^2 H_l}{\partial \eta^2} = \frac{1}{2} H_l + \frac{1}{2} \bar{\tau} \frac{\partial H_l}{\partial \bar{\tau}} - \frac{1}{2}(\eta + \dot{y}_m) \frac{\partial H_l}{\partial \eta} - \frac{1}{2} \dot{y}_m g''(\eta\bar{\tau}) - t_m \bar{\tau} g'''(\eta\bar{\tau}), \quad 0 < \eta < \infty, \tag{79}$$

where the dot now denotes differentiation with respect to $\bar{\tau}$, and the boundary and initial conditions are

$$t_m \bar{\tau} \frac{\partial G_s}{\partial \xi}\bigg|_{\xi=1} = -\frac{\kappa}{2} y_m \dot{y}_m G_s|_{\xi=1}, \qquad t_m \frac{\partial H_l}{\partial \eta}\bigg|_{\eta=0} = -\frac{1}{2} \dot{y}_m H_l|_{\eta=0} - \frac{\dot{y}_m}{2\bar{\tau}} g'(0) - t_m g''(0), \tag{80}$$

$$\beta t_m^{-1} \dot{y}_m = 2\bar{\tau}^2 H_l|_{\eta=0} - 2\bar{\tau} - 2K\bar{\tau} G_s|_{\xi=1}, \tag{81}$$

$$KG_s = -1 \quad \text{at } \xi = 0, \tag{82}$$

$$H_l \to 0 \quad \text{as } \eta \to \infty, \tag{83}$$

$$y_m(0) = 0. \tag{84}$$

Now, since $y_m \sim \bar{\tau}^3$ as $\bar{\tau} \to 0^+$, on setting $y_m = \alpha\bar{\tau}^3 + O(\bar{\tau}^3)$, where α is a constant to be determined, we have

$$\frac{\mathrm{d}^2 G_s}{\mathrm{d}\xi^2} = 0, \qquad t_m \frac{\mathrm{d}^2 H_l}{\mathrm{d}\eta^2} = \frac{1}{2} H_l - \frac{1}{2} \eta \frac{\mathrm{d}H_l}{\mathrm{d}\eta}, \tag{85}$$

subject to

$$\frac{\mathrm{d}G_s}{\mathrm{d}\xi}(1) = 0, \qquad G_s(0) = -\frac{1}{K}, \qquad H_l|_{\eta\to\infty} \to 0, \qquad \frac{\mathrm{d}H_l}{\mathrm{d}\eta}(0) = -g''(0), \tag{86}$$

in the limit as $\bar{\tau} \to 0^+$. These have the solutions

$$H_s = -\frac{1}{K}, \qquad H_l = g''(0)\left[e^{-\eta^2/\pi} - \eta\,\mathrm{erfc}\left(\frac{\eta}{\sqrt{\pi}}\right)\right], \tag{87}$$

where, from (81), the coefficient α satisfies

$$\alpha = \frac{2t_m g''(0)}{3\beta}, \tag{88}$$

which corresponds to the results in [8,10].

4.2. Discretization

4.2.1. Pre-solidification stage

Here, we solve Eq. (40) for $0 < \bar{\zeta} < 1, 0 < z < \infty$, subject to (41) and (43). In practice, a finite computational domain of extent z_∞ is used, although z_∞ must be large enough to ensure that the correct asymptotic behaviour as $z \to \infty$ is captured; since θ_l is known to decay exponentially as $z \to \infty, z_\infty = 10$ proves to be adequate. We use a uniform mesh with $I+1$ and $N+1$ points in z and $\bar{\zeta}$ variables, respectively; this gives spacings $\Delta z = z_\infty/I$ and $\Delta\bar{\zeta} = 1/N$, respectively.

To apply the box scheme, we rewrite (40) as a system of first-order equations:

$$\frac{\partial\theta_l}{\partial z} = U_l, \tag{89}$$

$$t_m\frac{\partial U_l}{\partial z} = \frac{1}{2}\left(\theta_l + \bar{\zeta}\frac{\partial\theta_l}{\partial\bar{\zeta}}\right) - \frac{z}{2}U_l. \tag{90}$$

For a general dependent variable C and general independent variables X and Y, we define the following finite difference operators:

$$\mu_X C_{i+\frac{1}{2}}^{n+\frac{1}{2}} = \frac{C_{i+\frac{1}{2}}^{n+1} + C_{i+\frac{1}{2}}^{n}}{2}, \qquad \delta_X C_{i+\frac{1}{2}}^{n+\frac{1}{2}} = \frac{C_{i+\frac{1}{2}}^{n+1} - C_{i+\frac{1}{2}}^{n}}{\Delta X} \tag{91}$$

$$\mu_Y C_{i+\frac{1}{2}}^{n+\frac{1}{2}} = \frac{C_{i+1}^{n+\frac{1}{2}} + C_{i}^{n+\frac{1}{2}}}{2}, \qquad \delta_Y C_{i+\frac{1}{2}}^{n+\frac{1}{2}} = \frac{C_{i+1}^{n+\frac{1}{2}} - C_{i}^{n+\frac{1}{2}}}{\Delta Y}. \tag{92}$$

With $X = \bar{\zeta}$, $Y = z$, the box scheme applied to Eqs. (89) and (90) therefore gives, for $n = 0, 1, 2, \ldots, N-1$, and dropping the subscript "l",

$$\mu_{\bar{\zeta}}\delta_z\theta_{i+\frac{1}{2}}^{n+\frac{1}{2}} = \mu_{\bar{\zeta}}\mu_z U_{i+\frac{1}{2}}^{n+\frac{1}{2}} \tag{93}$$

$$t_m\mu_{\bar{\zeta}}\delta_z U_{i+\frac{1}{2}}^{n+\frac{1}{2}} = \frac{1}{2}\left(\mu_{\bar{\zeta}}\mu_z\theta_{i+\frac{1}{2}}^{n+\frac{1}{2}} + \bar{\zeta}^{n+\frac{1}{2}}\mu_z\delta_{\bar{\zeta}}\theta_{i+\frac{1}{2}}^{n+\frac{1}{2}}\right) - \frac{1}{2}z_{i+\frac{1}{2}}\mu_{\bar{\zeta}}\mu_z U_{i+\frac{1}{2}}^{n+\frac{1}{2}}, \tag{94}$$

which holds for $i = 1, \ldots, I-1$. Note that, for brevity we have simply written $\bar{\zeta}^{n+\frac{1}{2}}$ and $z_{i+\frac{1}{2}}$ to denote $\mu_{\bar{\zeta}}\bar{\zeta}^{n+\frac{1}{2}}$ and $\mu_z z_{i+\frac{1}{2}}$, respectively. The same simplification is used for $\bar{\tau}$, ξ and η in the solidification stage discretizations described below.

The boundary conditions (41) and (42) give

$$U_0^n = 0, \tag{95}$$

$$\theta_M^n = 0, \tag{96}$$

respectively. Finally, (44) gives, for $i = 0, 1, \ldots, I$,

$$\theta_i^0 = 2\sqrt{\frac{t_m}{\pi}}\exp\left(-\frac{z_i^2}{4t_m}\right) - z_i\,\mathrm{erfc}\left(\frac{z_i}{2\sqrt{t_m}}\right), \qquad U_i^0 = -\mathrm{erfc}\left(\frac{z_i}{2\sqrt{t_m}}\right). \tag{97}$$

The discretized equations are written as a matrix system which can then be inverted to determine U_i^{n+1} and θ_i^{n+1}, for $i = 1, 2, \ldots, I$. We do, however, need to determine the value of the unknown t_m. This is done by solving the matrix system for some value of t_m up to $\bar{\zeta} = 1$ and seeing how well Eq. (45) is satisfied; based on the discrepancy, a new value of t_m and the matrix system resolved, with iterations being performed until Eq. (45) is satisfied to within a prescribed criterion. This procedure can be formally implemented in terms of a nonlinear solver, such as `fzero` in Matlab, with a suitable initial guess for t_m. The function `fzero` itself is based on a bisection algorithm, and is appropriate enough for this task; there is, therefore, no need to compute derivatives with respect to t_m. The computational cost depends on the initial guess for t_m, and examples are given in Table 1; the system is robust enough so that initial guesses 0.5 and 0.8, for example, both lead to the same prediction of t_m up to 16 decimal places. The CPU time has been calculated using Matlab's `tictoc` command. All computations were performed on a desktop with a 3 GHz Intel Xeon Dual-Core processor and 96 GB RAM.

Table 1
Dependence of function count, computed value of t_m and CPU time on the initial guess for t_m. Mesh values used are $\Delta z = 0.2$ and $\bar{\zeta} = 0.04$.

Initial guess for t_m	Function count	Computed value of t_m	CPU (s)
0.5	28	0.787895515367579	0.466468
0.6	23	0.787895515367579	0.385847
0.7	18	0.787895515367579	0.278032
0.8	6	0.787895515367579	0.104898
0.9	19	0.787895515367579	0.281816

4.2.2. Solidification stage

Considering the solid phase first, we write (78) as

$$\frac{\partial G_s}{\partial \xi} = \hat{G}, \tag{98}$$

$$t_m \bar{\tau} \frac{\partial \hat{G}}{\partial \xi} = \kappa y_m \left[\frac{1}{2} y_m \frac{\partial G_s}{\partial \bar{\tau}} - \frac{\xi}{2} \dot{y}_m \hat{G} \right], \tag{99}$$

which is then discretized, on dropping the subscript "s", as

$$\mu_{\bar{\tau}} \delta_{\xi} G_{i+\frac{1}{2}}^{n+\frac{1}{2}} = \mu_{\bar{\tau}} \mu_{\xi} \hat{G}_{i+\frac{1}{2}}^{n+\frac{1}{2}}, \tag{100}$$

$$t_m \bar{\tau}^{n+\frac{1}{2}} \mu_{\bar{\tau}} \delta_{\xi} \hat{G}_{i+\frac{1}{2}}^{n+\frac{1}{2}} = \kappa \mu_{\bar{\tau}} y_m^{n+\frac{1}{2}} \left[\frac{1}{2} \mu_{\bar{\tau}} y_m^{n+\frac{1}{2}} \mu_{\xi} \delta_{\bar{\tau}} G - \frac{1}{2} \xi_{i+\frac{1}{2}} \delta_{\bar{\tau}} y_m^{n+\frac{1}{2}} \mu_{\bar{\tau}} \mu_{\xi} \hat{G}_{i+\frac{1}{2}}^{n+\frac{1}{2}} \right], \tag{101}$$

for $i = 1, 2, \ldots, I_s - 1$ and $n = 0, 1, 2, \ldots$. As for the liquid phase, we write (79) as

$$\frac{\partial H_l}{\partial \eta} = \hat{H}, \tag{102}$$

$$t_m \frac{\partial \hat{H}}{\partial \eta} = \frac{1}{2} H_l + \frac{1}{2} \bar{\tau} \frac{\partial H_l}{\partial \bar{\tau}} - \frac{1}{2} (\eta + \dot{y}_m) \hat{H} - \frac{1}{2} \dot{y}_m g''(\eta \bar{\tau}) - t_m \bar{\tau} g'''(\eta \bar{\tau}), \tag{103}$$

which is then discretized, on dropping the subscript "l", as

$$\mu_{\bar{\tau}} \delta_{\eta} H_{i+\frac{1}{2}}^{n+\frac{1}{2}} = \mu_{\bar{\tau}} \mu_{\eta} \hat{H}_{i+\frac{1}{2}}^{n+\frac{1}{2}}, \tag{104}$$

$$\begin{aligned} t_m \mu_{\bar{\tau}} \delta_{\eta} \hat{H}_{i+\frac{1}{2}}^{n+\frac{1}{2}} \;=\; & \frac{1}{2} \mu_{\bar{\tau}} \mu_{\eta} H_{i+\frac{1}{2}}^{n+\frac{1}{2}} + \frac{1}{2} \bar{\tau}^{n+\frac{1}{2}} \mu_{\eta} \delta_{\bar{\tau}} H_{i+\frac{1}{2}}^{n+\frac{1}{2}} - \frac{1}{2} \left(\eta_{i+\frac{1}{2}} + \delta_{\bar{\tau}} y_m^{n+\frac{1}{2}} \right) \mu_{\bar{\tau}} \mu_{\eta} \hat{H}_{i+\frac{1}{2}}^{n+\frac{1}{2}} \\ & - \frac{1}{2} \delta_{\bar{\tau}} y_m^{n+\frac{1}{2}} \mu_{\bar{\tau}} \mu_{\eta} \hat{V}_{i+\frac{1}{2}}^{n+\frac{1}{2}} - t_m \bar{\tau}^{n+\frac{1}{2}} \mu_{\bar{\tau}} \mu_{\eta} \hat{W}_{i+\frac{1}{2}}^{n+\frac{1}{2}}, \end{aligned} \tag{105}$$

for $i = 1, 2, \ldots, I_l - 1$ and $n = 0, 1, 2, \ldots$. Note that $\hat{V}$ and $\hat{W}$ represent the values of $V_l(z, 1)$ $(= g''(z))$ and $W_l(z, 1)$ $(= g'''(z))$ from the pre-solidification stage, but interpolated to account for the fact that z is replaced by $\eta \bar{\tau}$. Boundary conditions (80)–(82) are now

$$t_m \bar{\tau}^{n+\frac{1}{2}} \mu_{\bar{\tau}} \hat{G}_{I_s}^{n+\frac{1}{2}} = -\frac{\kappa}{2} \mu_{\bar{\tau}} y_m^{n+\frac{1}{2}} \delta_{\bar{\tau}} y_m^{n+\frac{1}{2}} \mu_{\bar{\tau}} G_{I_s}^{n+\frac{1}{2}}, \tag{106}$$

$$t_m \bar{\tau}^{n+\frac{1}{2}} \mu_{\bar{\tau}} \hat{H}_0^{n+\frac{1}{2}} = -\frac{1}{2} \bar{\tau}^{n+\frac{1}{2}} \delta_{\bar{\tau}} y_m^{n+\frac{1}{2}} H_0^{n+\frac{1}{2}} - \frac{1}{2} \delta_{\bar{\tau}} y_m^{n+\frac{1}{2}} g'(0) - t_m \bar{\tau}^{n+\frac{1}{2}} g''(0), \tag{107}$$

$$\beta t_m^{-1} \mu_{\bar{\tau}} y_m^{n+\frac{1}{2}} = 2 \left(\bar{\tau}^{n+\frac{1}{2}} \right)^2 \mu_{\bar{\tau}} H_0^{n+\frac{1}{2}} - 2 \bar{\tau}^{n+\frac{1}{2}} - 2K \bar{\tau}^{n+\frac{1}{2}} \mu_{\bar{\tau}} G_{I_s}^{n+\frac{1}{2}}, \tag{108}$$

$$K \mu_{\bar{\tau}} G_0^{n+\frac{1}{2}} = -1, \tag{109}$$

$$\mu_{\bar{\tau}} H_{I_l}^{n+\frac{1}{2}} = 0, \tag{110}$$

whereas the initial conditions become

$$y_m^0 = 0, \tag{111}$$

$$G_i^0 = -\frac{1}{K}, \quad i = 0, \ldots, I_s, \tag{112}$$

$$H_i^0 = g''(0) \left[e^{-\eta_i^2/\pi} - \eta_i \operatorname{erfc} \left(\frac{\eta_i}{\sqrt{\pi}} \right) \right], \quad i = 0, \ldots, I_l. \tag{113}$$

4.3. Order of accuracy

We will also wish to determine the order of accuracy of the scheme and of the solution. We start this discussion by considering a sequence ΔY_k where

$$\Delta Y_k = 2^{-k}\Delta Y_0, \quad k = 1, 2, \ldots,$$

and denote the space coordinates of meshes associated with this sequence by

$$Y_{i,k} = i\Delta Y_k, \quad i = 0, 1, \ldots, I_k, k = 0, 1, 2, \ldots,$$

where

$$I_k = 2^k I_0, \quad k = 1, 2, \ldots.$$

As discussed in [12], for a general numerical solution $F^n_{2^k i}$ and corresponding exact solution $f(Y_{i,k}, t^n)$ at the nth time step, t^n, the error and corresponding order of convergence, $E^n_{F,k}$ and $p_{F,k}$ respectively, are given by

$$E^n_{F,k} = \left(\Delta Y_k \sum_{i=0}^{I_0}\left(f(Y_{i,0}, t^n) - F^n_{2^k i}\right)^2\right)^{1/2}, \qquad p_{F,k} = \frac{\ln(E^n_{F,k}/E^n_{F,k+1})}{\ln 2}, \tag{114}$$

for $k = 0, 1, 2, \ldots$; furthermore, the accuracy of the solution with respect to F, p_F, is then

$$p_F = \lim_{k\to\infty} p_{F,k}. \tag{115}$$

As for the accuracy of the scheme with respect to F, $\bar{p}_F$, we first define

$$\bar{E}^n_{F,k} = \left(\sum_{i=0}^{I_0}\left(F^n_{2^k i} - F^n_{2^{k-1} i}\right)^2\right)^{1/2}, \qquad \bar{p}_{F,k} = \ln(\bar{E}^n_{F,k}/\bar{E}^n_{F,k+1})/\ln 2, \tag{116}$$

for $k = 1, 2, \ldots$; then,

$$\bar{p}_F = \lim_{k\to\infty} \bar{p}_{F,k}. \tag{117}$$

In cases where an exact solution was known and there were no discontinuities in the boundary conditions after reformulation, Mitchell and Vynnycky [7] showed that $p_F = \bar{p}_F$. Furthermore, Mitchell et al. [10] demonstrated that it was also possible to apply this idea to the spatial derivative of F and the location of the moving boundary, which we denote as s for the purpose of this discussion; thus, we set, for $k = 0, 1, 2, \ldots,$

$$E^n_{V,k} = \left(\Delta Y_k \sum_{i=0}^{I_0}\left(v(Y_{i,0}, t^n) - V^n_{2^k i}\right)^2\right)^{1/2}, \qquad p_{V,k} = \frac{\ln(E^n_{V,k}/E^n_{V,k+1})}{\ln 2}, \tag{118}$$

$$E^n_{s,k} = |s^n_k - s(t^n)|, \quad k = 0, 1, 2, \ldots, \qquad p_{s,k} = \frac{\ln(E^n_{s,k}/E^n_{s,k+1})}{\ln 2}, \tag{119}$$

where $v = \partial f/\partial y$, and

$$\bar{E}^n_{V,k} = \left(\sum_{i=0}^{I_0}\left(V^n_{2^k i} - V^n_{2^{k-1} i}\right)^2\right)^{1/2}, \qquad \bar{p}_{V,k} = \frac{\ln(\bar{E}^n_{V,k}/\bar{E}^n_{V,k+1})}{\ln 2}, \tag{120}$$

$$\bar{E}^n_{s,k} = |s^n_k - s^n_{k-1}|, \quad k = 1, 2, \ldots, \qquad \bar{p}_{s,k} = \frac{\ln(\bar{E}^n_{s,k}/\bar{E}^n_{s,k+1})}{\ln 2}, \tag{121}$$

for $k = 1, 2, \ldots$.

As it stands, the above discussion applies to moving boundary problems for which there is only one phase. In order to ensure that this type of accuracy test can be carried out for our current problem, it is clear that we need to extend this to situations with multiple phases and where the number of phases varies with time. In principle, there is no problem in making this extension, provided that

$$\Delta\bar{\tau} = \Delta\bar{\xi}, \qquad \Delta\xi = \Delta\eta = \Delta z;$$

however, there turn out to be other factors to consider.

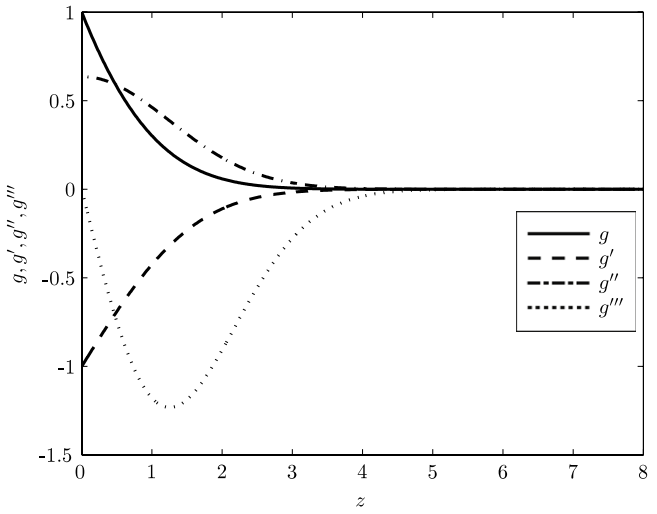

Fig. 2. g, g', g'', g''' vs. z.

4.4. Further considerations

The fact that g is not constant, which manifests itself in the third and fourth terms on the right-hand side of Eq. (103), leads to several inter-related numerical issues that must be treated; the ensuing discussion is along the lines of that in [13], where these issues were resolved for the case of a fixed-boundary problem. First of all, although it is clear that, in practice, a finite computational domain of extent η_∞ has to be chosen, considerably greater care must be taken regarding this choice than in earlier work in order to ensure that the correct asymptotic behaviour is captured as $\eta \to \infty$. If g is constant, so that the derivatives of g are zero, then since H is known to decay exponentially as $\eta \to \infty$, $\eta_\infty = 10$ proves to be large enough. However, when g is not constant, it is necessary to know how it decays as $z \to \infty$, since this decay must be correctly reflected in the discretized version of Eq. (103); for reference, this is shown for g, g', g'' and g''' in Fig. 2. Since $z = \eta\bar{\tau}$, this means that if the value of η_∞ is too small, then the asymptotic decay of g and its derivatives will not be captured in the numerical solution; so, it appears, at first sight, necessary to take

$$\eta_\infty \Delta\bar{\tau} \gg 1. \tag{122}$$

However, the process of determining the accuracy, as described in [12] and applied below, relies on decreasing the value of $\Delta\tau$, and it is evident that as k increases, inequality (122) will no longer be satisfied, no matter how large we take η_∞. In fact, there turns out to be a tidy resolution to this particular issue. Because the accuracy check requires that solutions are computed numerically for meshes that have different $\Delta\eta$, it does not require η_∞ be the same for each refinement; consequently, if we double η_∞ and increase I_l fourfold, then we will simultaneously halve the size of $\Delta\eta$—exactly what is necessary when performing accuracy checks for problems posed on finite domains.

The present case revolves around what happens if g, g', g'' and g''' have been computed as a result of numerical integration up to $t = t_m$. This leads to a dilemma as to what to use for g, g', g'' and g''' or rather $g(\eta\bar{\tau}), g'(\eta\bar{\tau}), g''(\eta\bar{\tau})$ and $g'''(\eta\bar{\tau})$ in Eq. (103), since $g(\eta_i\bar{\tau}_n)$ will not have been computed for all the values of η_i and $\bar{\tau}_n$ at which it is required. One of the appealing features of the double-deck schemes in [11,14] was that this issue was resolved simply by dropping points systematically from the upper deck; thus, there was no need to introduce new arbitrary points. Here, we adopt a different approach: when g is required at $(\eta_i, \bar{\tau}_n)$, we interpolate the value of $g(\eta_i\bar{\tau}_n)$ from $(g_i)_{i=0,\ldots,I}$ if $\eta_i\bar{\tau}_n < z_I$; otherwise, if $\eta_i\bar{\tau}_n\eta_i \geq z_I$, we set $g(\bar{\tau}_n\eta_i) = g_I$. As we will show in Section 5, this turns out to have no adverse effects on the accuracy of the scheme.

5. Results

5.1. Pre-solidification stage

First, we consider the numerical accuracy of the three schemes used for the pre-solidification stage. Tables 2–4 compare the values of $E^n_{T_l,k}$, $E^n_{U_l,k}$, $E^n_{V_l,k}$ and $E^n_{W_l,k}$ and p at $\bar{\zeta} = 1$ for a sequence of progressively finer meshes. As is evident, from these tables, we find that $p = 2$ for all of these cases, as expected. Note that second order convergence for t_m is also given in Table 2.

Table 2
Comparison of the order of accuracy of the numerical solution, solving (40), (41) and (44) at $\bar{\zeta} = 1$, with $\Delta\bar{\zeta}/\Delta z = 0.2$ and $z_\infty = 8$.

$\Delta z(k)$	Results for t_m		Results for T_l		Results for U_l	
	Absolute error	Order, p	E^n	Order, p	E^n	Order, p
$1/2(k=0)$	1.55×10^{-2}		3.13×10^{-3}		2.73×10^{-3}	
$1/4(k=1)$	3.90×10^{-3}	1.99277	7.63×10^{-4}	2.03730	6.59×10^{-4}	2.05174
$1/8(k=2)$	9.76×10^{-4}	1.99821	1.90×10^{-4}	2.00938	1.63×10^{-4}	2.01175
$1/16(k=3)$	2.44×10^{-4}	1.99955	4.73×10^{-5}	2.00235	4.07×10^{-5}	2.00287
$1/32(k=4)$	6.10×10^{-5}	1.99989	1.18×10^{-5}	2.00059	1.02×10^{-5}	2.00071

Table 3
Comparison of the order of accuracy of the numerical solution, solving (46)–(49) at $\bar{\zeta} = 1$, with $\Delta\bar{\zeta}/\Delta z = 0.2$ and $z_\infty = 8$.

$\Delta z(k)$	Results for U_l		Results for V_l	
	E^n	Order, p	E^n	Order, p
$1/2(k=0)$	5.50×10^{-3}		8.74×10^{-3}	
$1/4(k=1)$	1.37×10^{-3}	2.00322	2.01×10^{-3}	2.12235
$1/8(k=2)$	3.43×10^{-4}	2.00081	4.82×10^{-4}	2.05883
$1/16(k=3)$	8.58×10^{-5}	2.00020	1.18×10^{-4}	2.02928
$1/32(k=4)$	2.14×10^{-5}	2.00005	2.92×10^{-5}	2.01465

Table 4
Comparison of the order of accuracy of the numerical solution, solving (50)–(53) at $\bar{\zeta} = 1$, with $\Delta\bar{\zeta}/\Delta z = 0.2$ and $z_\infty = 8$.

$\Delta z(k)$	Results for V_l		Results for W_l	
	E^n	Order, p	E^n	Order, p
$1/2(k=0)$	1.25×10^{-2}		1.67×10^{-2}	
$1/4(k=1)$	2.96×10^{-3}	2.07430	4.12×10^{-3}	2.01467
$1/8(k=2)$	7.16×10^{-4}	2.04800	1.03×10^{-3}	2.00313
$1/16(k=3)$	1.75×10^{-4}	2.02683	2.57×10^{-4}	2.00075
$1/32(k=4)$	4.35×10^{-5}	2.01414	6.42×10^{-5}	2.00019

Table 5
Comparison of the order of accuracy of the numerical scheme, solving (100)–(113) at $\bar{\tau} = 1$, with $\Delta\bar{\zeta}/\Delta z = \Delta\bar{\tau}/\Delta\xi = \Delta\bar{\tau}/\Delta\eta = 0.2$, $z_\infty = 8$ and $\eta_\infty = 50$.

Δz, $\Delta\xi$, $\Delta\eta$ (k)	Results in the solid		Results in the liquid		
	$\bar{p}$ (for G)	$\bar{p}$ (for $\hat{G}$)	$\bar{p}$ (for H)	$\bar{p}$ (for $\hat{H}$)	$\bar{p}$ (for y_m)
$1/20(k=2)$	2.12173	2.84264	5.68467	5.68338	4.08113
$1/40(k=3)$	2.01109	2.00602	2.09088	2.09080	1.96723
$1/80(k=4)$	2.00240	2.00138	2.02132	2.02129	1.99173
$1/160(k=5)$	2.00054	2.00031	2.00374	2.00359	1.99815

5.2. Solidification stage

Table 5 shows the values of $\bar{p}$ for G, $\hat{G}$, H, $\hat{H}$ and y_m at $\bar{\tau} = 1$; here, we see convincing evidence that $\bar{p} = 2$ for all variables, which is the key result of this work. Note that this problem corresponds to the case D considered in [13], albeit now for a moving-boundary problem rather than a fixed-boundary problem, since we have

$$\lim_{t \to t_m^+} T_l(y,t) = \lim_{y \to 0} T_l(y, t_m),$$

$$\lim_{t \to t_m^+} \frac{\partial T_l}{\partial y}(y,t) = \lim_{y \to 0} \frac{\partial T_l}{\partial y}(y, t_m),$$

i.e. there is no inconsistency in either T_l or $\partial T_l/\partial y$ as $y \to 0$, $t \to t_m^+$, as indicated earlier.

As in [13], it is perhaps, at first sight, surprising that we have managed to obtain $\bar{p} = 2$ for all variables in Table 5, even though inequality (122) is not satisfied on the finest mesh. The reason appears to be that the equation being solved, namely (103), contains

$$\frac{1}{\pi}\left(\frac{3}{2}\alpha - \eta\right)\bar{\tau}^2 e^{-\eta^2\bar{\tau}^2/\pi},$$

rather than just $\exp\left(-\bar{\tau}^2\eta^2\right)$; consequently, as $\Delta\bar{\tau}$ is decreased, the size of this source term decreases. It is evident that the largest value that this term can take – and hence which the method neglects, because of the finiteness of the computational

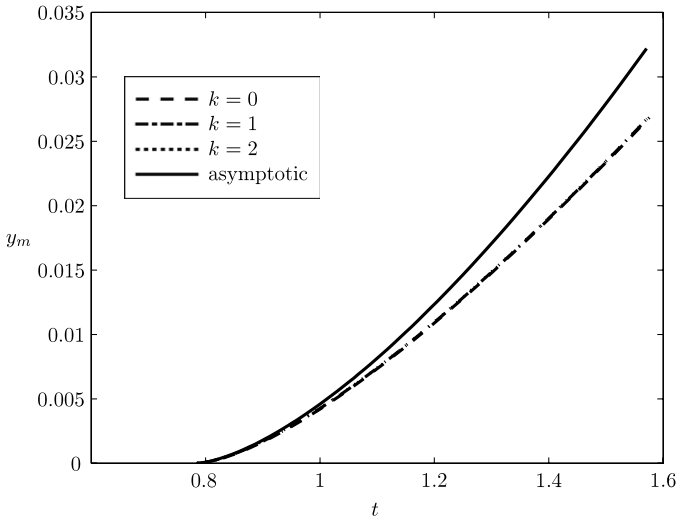

Fig. 3. y_m against t for the meshes corresponding to $k = 0, 1, 2$. The dashed line is the asymptotic solution as $t \to t_m^+$.

Table 6
Data used to generate Fig. 3, in tabulated form.

t	$k = 0$	$k = 1$	$k = 2$	Asymptotic
0.7878955154	0	0.0000035879	0.0000051752	0.0000052380
0.7891561482	0.0000015513	0.0000078625	0.0000098952	0.0000099959
0.7929380467	0.0000154403	0.0000260889	0.0000290542	0.0000293400
0.7992412108	0.0000538379	0.0000690902	0.0000731725	0.0000740470
0.8080656408	0.0001286761	0.0001485456	0.0001538217	0.0001561901
0.8194113360	0.0002515902	0.0002760026	0.0002825209	0.0002880884
0.8332782971	0.0004338707	0.0004627028	0.0004705017	0.0004821234
0.8496665238	0.0006864169	0.0007195075	0.0007286215	0.0007506969
0.8685760161	0.0010196975	0.0010568524	0.0010673130	0.0011062192
0.8900067742	0.0014437200	0.0014847132	0.0014965496	0.0015611042
0.9139587978	0.0019680059	0.0020125827	0.0020258214	0.0021277680
0.9404320871	0.0026015760	0.0026494550	0.0026641201	0.0028186277
0.9694266421	0.0033529407	0.0034038182	0.0034199312	0.0036461010
1.0009424627	0.0042300995	0.0042836537	0.0043012340	0.0046226060
1.0349795490	0.0052405444	0.0052964410	0.0053155068	0.0057605612
1.0715379009	0.0063912706	0.0064491687	0.0064697374	0.0070723852
1.1106175185	0.0076887903	0.0077483485	0.0077704384	0.0085704966
1.1522184017	0.0091391514	0.0092000337	0.0092236641	0.0102673141
1.1963405505	0.0107479570	0.0108098389	0.0108350318	0.0121752568
1.2429839650	0.0125203894	0.0125829627	0.0126097429	0.0143067434
1.2921486452	0.0144612330	0.0145242104	0.0145526068	0.0166741928
1.3438345910	0.0165748998	0.0166380177	0.0166680633	0.0192900240
1.3980418025	0.0188654528	0.0189284743	0.0189602068	0.0221666561
1.4547702796	0.0213366319	0.0213993473	0.0214328089	0.0253165079
1.5140200223	0.0239918758	0.0240541035	0.0240893407	0.0287519983
1.5757910307	0.0268343466	0.0268959300	0.0269329944	0.0324855463

domain – occurs when $\bar{\tau} = \pi^{1/2}/\eta_\infty$ and is equal to

$$\left(\frac{3}{2}\alpha - \eta_\infty\right)\frac{1}{\eta_\infty^2 e}.$$

Thus, in Table 5, this appears to be small enough to ensure $\bar{p}$ converges to 2. As a corollary, we can note this as being a further positive side-effect of using similarity-like variables rather than the original physical variables, even though the problem does not actually have a similarity solution.

Lastly, Fig. 3 shows y_m as a function of t for three different meshes; we have also included the solution $y_m = \alpha\,(t - t_m)^{3/2}$, which is valid as $t \to t_m^+$. This figure demonstrates how the analytical profile diverges from the numerical solutions as t increases, and also that the numerical solutions for the three meshes are virtually indistinguishable from other; the data used to generate Fig. 3 is tabulated in Table 6, and the CPU times required to generate solutions for $k = 0, 1, \ldots, 5$ are given in Table 7.

Table 7
CPU times required to generate solutions for $k = 0, 1, 2, \ldots, 4$.

	k				
	0	1	2	3	4
CPU (s)	4	28	251	2156	23 275

6. Conclusions

In this paper, we have considered the solidification due to a cooling heat flux of material that is initially above its melting temperature. Using earlier analysis which demonstrated that the front starts to grow as $(t - t_m)^{3/2}$, the Keller box finite-difference scheme and the so-called boundary immobilization method were coupled together to yield a numerical scheme which maintains second-order accuracy in time and space variables, in spite of a discontinuity in the boundary conditions.

Although this paper has considered explicitly the case of a heat-flux (Neumann) cooling condition, the appropriate analysis for the case when a convective cooling (Robin) condition will be qualitatively similar; in particular, we expect to find that the front grows as $(t - t_m)^{3/2}$. Furthermore, the analysis presented here also forms the basis for analysing melting and solidification problems in finite slabs, as considered recently by Roday and Kazmierczak [4–6] using heat-balance integral methods.

A particular practical application of this method is to models for continuous casting processes [15–19]; although these models are neither one-dimensional, nor transient, the spatial coordinate along the direction of casting acts as a time-like variable, with the casting velocity as a constant of proportionality, and with t_m being proportional to the distance from the inlet along the mould wall at which molten metal begins to solidify. Since casting geometries are typically slender, a planar two-dimensional, or axisymmetric, steady state model can be reformulated as a one-dimensional transient model, as in this paper.

Acknowledgments

The authors acknowledge the support of the Mathematics Applications Consortium for Science and Industry (www.macsi.ul.ie) funded by the Science Foundation Ireland Mathematics Initiative Grant 06/MI/005.

Appendix. Behaviour of y_m as $t \to t_m^+$

Returning to Eqs. (12)–(21), we now change variables by setting

$$\eta = \begin{cases} y/y_m, & y < y_m \\ 1 + y - y_m, & y \geq y_m, \end{cases} \tag{A.1}$$

with

$$T_s = y_m F, \quad 0 \leq \eta < 1, t > t_m \tag{A.2}$$

$$T_l = G, \quad 1 \leq \eta \leq \infty, t > 0. \tag{A.3}$$

Then, in the pre-solidification stage, when $0 \leq t \leq t_m$, we solve

$$G_{\eta\eta} = G_t, \quad 1 < \eta < \infty, \tag{A.4}$$

subject to

$$G = -1 \quad \text{at } t = 0, \tag{A.5}$$

$$G_\eta = -\mathcal{Q}(t) \quad \text{at } \eta = 1, \tag{A.6}$$

$$G \to -1 \quad \text{as } \eta \to \infty. \tag{A.7}$$

This stage ends when $G(1, t) = 0$ which gives t_m. For the solidification stage, when $t > t_m$, we solve

$$F_{\eta\eta} = \kappa y_m \left[\dot{y}_m F + y_m F_t - \eta \dot{y}_m F_\eta\right] \quad 0 < \eta < 1, \tag{A.8}$$

$$G_{\eta\eta} = G_t - \dot{y}_m G_\eta \quad 1 < \eta < \infty, \tag{A.9}$$

subject to

$$F = G = 0 \quad \text{at } \eta = 1, \tag{A.10}$$

$$\beta \dot{y}_m = G_\eta - K F_\eta \quad \text{at } \eta = 1, \tag{A.11}$$

$$K F_\eta = -\mathcal{Q}(t) \quad \text{at } \eta = 0, \tag{A.12}$$

$$G \to -1 \quad \text{as } \eta \to \infty, \tag{A.13}$$

$$y_m = 0 \quad \text{at } t = t_m. \tag{A.14}$$

Suppose that y_m has the form

$$y_m \sim \lambda(t - t_m)^\alpha + o(t - t_m)^\alpha, \tag{A.15}$$

where α and λ are positive constants that are to be determined. Also, from (A.8), this will require

$$F = F_0(\eta) + (t - t_m)^{2\alpha-1} F_1(\eta) + o(t - t_m)^{2\alpha-1}; \tag{A.16}$$

however, it is now not possible for the term from the solid region to participate in the order balance for the Stefan condition (60) at the next highest order, i.e. $(t - t_m)^{\alpha-1}$, since this would need $\alpha = 0$. An alternative would be to miss out the contribution of the solid region completely at this order, which requires $\alpha > 1$; in any case, it is necessary to know the behaviour of G as $t \to t_m^+$. Setting for convenience $\zeta = t - t_m$ and $\xi = \eta - 1$, and then using the form of y_m in (A.15) we consider the solution to

$$G_\zeta - \lambda\alpha\zeta^{\alpha-1} G_\xi = G_{\xi\xi}, \quad 0 < \xi < \infty, \zeta > 0, \tag{A.17}$$

subject to the boundary conditions

$$G(0, \zeta) = 0, \tag{A.18}$$

$$G \to -1 \quad \text{as } \xi \to \infty, \tag{A.19}$$

and the initial condition

$$G(\xi, 0) = G_o(\xi), \tag{A.20}$$

where $G_o(0) = 0$ and $G_o(\infty) = -1$. For the case when $\lambda = 0$, a closed-form expression in integral form is given by Carslaw and Jaeger [20]. Their analysis, which is based on the use of Fourier transforms defined for $-\infty < \xi < \infty$, can be exploited here even when $\lambda \neq 0$; we omit the majority of the details and quote the solution for G as

$$G(\xi, \zeta) = \frac{1}{2}\sqrt{\frac{1}{\pi\zeta}} \int_0^\infty G_o(\xi') \left\{ \exp\left(-\frac{(\xi + \lambda\zeta^\alpha - \xi')^2}{4\zeta}\right) - \exp\left(-\frac{(\xi - \lambda\zeta^\alpha + \xi')^2}{4\zeta}\right) \right\} \mathrm{d}\xi'. \tag{A.21}$$

Now, setting $\phi = (\xi' - \lambda\zeta^\alpha)/2\zeta^{1/2}$ and using (A.21), we have

$$(G_\xi)_{\xi=0} = 2\sqrt{\frac{1}{\pi\zeta}} \int_{-\lambda\zeta^\alpha/(2\sqrt{\zeta})}^\infty G_o(\Phi)\, \phi e^{-\phi^2}\, \mathrm{d}\phi, \tag{A.22}$$

where $\Phi = 2\phi\sqrt{\zeta} + \lambda\zeta^\alpha$. Expanding G_o as

$$G_o(\Phi) \approx G_o(0) + \Phi G_{o\xi}(0) + \frac{\Phi^2}{2} G_{o\xi\xi}(0) + O\left(\Phi^3\right), \tag{A.23}$$

and using the fact that $G_o(0) = 0$, means that (A.22) becomes

$$(G_\xi)_{\xi=0} = 2\sqrt{\frac{\kappa}{\pi\zeta}} G_{o\xi}(0) \int_{-\lambda\zeta^\alpha/(2\sqrt{\zeta})}^\infty \Phi\phi e^{-\phi^2}\, \mathrm{d}\phi + \sqrt{\frac{\kappa}{\pi\zeta}} G_{o\xi\xi}(0) \int_{-\lambda\zeta^\alpha/(2\sqrt{\zeta})}^\infty \Phi^2 \phi e^{-\phi^2}\, \mathrm{d}\phi + \cdots. \tag{A.24}$$

Calculating these integrals leads to the expression

$$\begin{aligned}(G_\xi)_{\xi=0} = {} & G_{o\xi}(0)\mathrm{erfc}\left(-\frac{\lambda\zeta^\alpha}{2\sqrt{\zeta}}\right) \\ & + G_{o\xi\xi}(0)\left[2\sqrt{\frac{\zeta}{\pi}}\left(1 + \frac{\lambda^2\zeta^{2\alpha-1}}{4}\right)\exp\left(-\frac{\lambda^2\zeta^{2\alpha-1}}{4}\right) + \lambda\zeta^\alpha \mathrm{erfc}\left(-\frac{\lambda\zeta^\alpha}{2\sqrt{\zeta}}\right)\right] + \cdots.\end{aligned} \tag{A.25}$$

If we expand (A.25) for small ζ we obtain

$$(G_\xi)_{\xi=0} \approx G_{o\xi}(0)\left(1 + \frac{\lambda}{2}\zeta^{\alpha-1/2} + \cdots\right) + 2\sqrt{\frac{\zeta}{\pi}} G_{o\xi\xi}(0) + \cdots. \tag{A.26}$$

Since we are assuming that $\alpha > 1$, we must have

$$(G_\xi)_{\xi=0} - G_{o\xi}(0) \sim \frac{2}{\sqrt{\pi}} G_{o\xi\xi}(0)\zeta^{1/2}.$$

Hence, from the Stefan condition, Eq. (A.11), we have, at leading order,

$$\beta\alpha\lambda(t - t_m)^{\alpha-1} = \frac{2}{\sqrt{\pi}} G_{o\xi\xi}(0)(t - t_m)^{1/2}, \tag{A.27}$$

from which we can deduce that $\alpha = 3/2$ and so

$$\lambda = \frac{4G_{o\xi\xi}(0)}{3\beta\sqrt{\pi}}. \tag{A.28}$$

References

[1] A.M.C. Chan, P. Smereka, M. Shoukri, An approximate analytical solution to the freezing problem subject to convective cooling and with arbitrary initial liquid temperatures, Int. J. Heat Mass Trans. 26 (1983) 1712–1715.
[2] C.J. Lozano, R. Reemsten, On a Stefan problem with an emerging free boundary, Num. Heat Trans. 4 (1981) 239–245.
[3] J. Ma, B.-X. Wang, The penetration of solid–liquid phase-change heat transfer interface with different kinds of boundary conditions, Int. J. Heat Mass Trans. 38 (1995) 2135–2138.
[4] A.P. Roday, M.J. Kazmierczak, Analysis of phase-change in finite slabs subjected to convective boundary conditions: part I – melting, Int. Rev. Chem. Engng. (Rapid Commun.) 1 (2009) 87–99.
[5] A.P. Roday, M.J. Kazmierczak, Analysis of phase-change in finite slabs subjected to convective boundary conditions: part II – freezing, Int. Rev. Chem. Engng. (Rapid Commun.) 1 (2009) 100–108.
[6] A.P. Roday, M.J. Kazmierczak, Melting and freezing in a finite slab due to a linearly decreasing free-stream temperature of a convective boundary condition, Thermal Sci. 2 (2009) 141–153.
[7] S.L. Mitchell, M. Vynnycky, Finite-difference methods with increased accuracy and correct initialization for one-dimensional Stefan problems, Appl. Math. Comput. 215 (2009) 1609–1621.
[8] M. Vynnycky, S.L. Mitchell, On the solution of Stefan problems with delayed onset of phase change, in: Proceedings of the 7th HEFAT Conference, Antalya, Turkey, 2010, pp. 709–714 (CD-ROM).
[9] S.L. Mitchell, M. Vynnycky, An accurate finite-difference method for ablation-type problems, J. Comput. Appl. Math. 236 (2012) 4181–4192.
[10] S.L. Mitchell, M. Vynnycky, I.G. Gusev, S.S. Sazhin, An accurate numerical solution for the transient heating of an evaporating droplet, Appl. Math. Comput. 217 (2011) 9219–9233.
[11] M. Vynnycky, Concerning closed-streamline flows with discontinuous boundary conditions, J. Engng. Math. 33 (1998) 141–156.
[12] J.C. Strikwerda, Finite Difference Schemes and Partial Differential Equations, 2nd edn, Society for Industrial Mathematics, 2004.
[13] M. Vynnycky, S.L. Mitchell, On the accuracy of a finite-difference method for parabolic PDEs with discontinuous boundary conditions, Num. Heat. Trans. B 64 (2013) 275–292.
[14] F.T. Smith, Boundary-layer flow near a discontinuity in wall conditions, J. Inst. Math. Appl. 13 (1974) 127–145.
[15] M. Vynnycky, On the role of radiative heat transfer in air gaps in vertical continuous casting, Appl. Math. Mod. 37 (2013) 2178–2188.
[16] M. Vynnycky, Air gaps in vertical continuous casting in round moulds, J. Engng. Math. 68 (2010) 129–152.
[17] J. Åberg, M. Vynnycky, H. Fredriksson, Heat-flux measurements of industrial on-site continuous copper casting and their use as boundary conditions for numerical simulations, Trans. Ind. Inst. Metals 62 (2009) 443–446.
[18] M. Vynnycky, A mathematical model for air-gap formation in vertical continuous casting: the effect of superheat, Trans. Ind. Inst. Metals 62 (2009) 495–498.
[19] M. Vynnycky, An asymptotic model for the formation and evolution of air gaps in vertical continuous casting, Proc. R. Soc. A 465 (2009) 1617–1644.
[20] H. Carslaw, J.C. Jaeger, Conduction of Heat in Solids, Clarendon Press, Oxford, 1959.